Earth and Planetary Science Letters 397 (2014) 93–100

Contents lists available at ScienceDirect

Earth and Planetary Science Letters

www.elsevier.com/locate/epsl

Feedbacks between flow, sediment motion and microbial growth on sand bars initiate and shape elongated stromatolite mounds

G. Mariotti *, J.T. Perron, T. Bosak

Department of Earth, Atmospheric and Planetary Sciences, MIT, Cambridge, MA, United States

ARTICLE INFO

Article history:
Received 31 October 2013
Received in revised form 15 April 2014
Accepted 22 April 2014
Available online 8 May 2014
Editor: G. Henderson

Keywords:
microbial mats
biostabilization
waves
ripples
platform
stromatolite morphology

ABSTRACT

Elongated stromatolites are often used as indicators of current direction and shoreline orientation, especially in paleoenvironmental reconstructions. However, mechanisms that create shore-parallel, m-scale elongated stromatolite mounds in carbonate sand are not well understood. We propose that this geometry is initiated by microbial growth on the parts of sand bars that experience low wave-induced bed shear stresses. We test this idea by growing microbial mats on carbonate sand bars in a laboratory wave tank. Cyanobacterial mats grow on the bar runnels, where sediment motion is negligible, but are absent from the bar ridges, where the waves generate migrating ripples. When microbially-promoted lithification reinforces and preserves this initial pattern, elongated stromatolites should initiate in the runnels of sand bars, with long wavelengths (5–100 m) and small width-to-wavelength ratios (~0.3). These dimensions are consistent with modern shore-parallel stromatolites in Hamelin Pool, Western Australia, and with patterns of microbial colonization in other sandy sediments. This model of elongated stromatolite mounds can inform paleoenvironmental reconstructions by clarifying and quantifying feedbacks among waves, sediment transport and microbial growth.

1. Introduction

Stromatolites are laminated sedimentary structures that exhibit a variety of macroscopic shapes, including domes, cones, clubs, cylinders, sheets and elongated mounds. Most columnar and elongated stromatolite morphologies larger than a centimeter have accreted in the presence of waves, currents and moving sediments (Altermann, 2008; Bosak et al., 2013a; Sakurai et al., 2005). However, it is not clear whether and how the sizes, shapes and spacings of these stromatolites reflect interactions between waves, currents, sediment motion and the growth of microbial mats, nor is it clear how microbes and stromatolites grow in areas where sediments are often mobilized (Bosak et al., 2013a; Tice et al., 2011; Gebelein, 1969).

Stromatolites with an elongated form present an especially intriguing case of interactions between microbial growth and the physical environment. If the factors that generate this elongated form are understood, elongated stromatolites could be used to infer the orientations of paleoshorelines, the directions of current-dominated and wave-dominated flows, and the feedbacks between microbial growth, hydrodynamic conditions and sedimentary landscapes in carbonate systems through time (Bosak et al., 2013b). For example, ancient marine stromatolites from upper intertidal areas are often elongated perpendicular to the shore, and are thought to be shaped by currents that drain the tidal platform (Logan, 1961; Hoffman, 1967, 1974; Gebelein, 1969; Playford, 1980; Truswell and Eriksson, 1973; Eriksson and Truswell, 1974). The formation of ancient shore-parallel elongated stromatolites has similarly been attributed to shore-parallel currents (Young and Jefferson, 1975; Young and Long, 1976; Jefferson and Young, 1989), even though modern stromatolite-forming environments offer little evidence of these currents.

Stromatolites forming in modern environments are particularly useful for understanding the environmental conditions and factors that shape stromatolites. Hamelin Pool, a ~20 km wide hypersaline embayment in Western Australia (Jahnert and Collins, 2013), harbors stromatolites that form by trapping and binding sand and by microbial precipitation of carbonate minerals (Reid et al., 2000). Large cylindrical stromatolites have grown on steeper platforms (slope of 40 m/km) at headlands (Fig. 1C), whereas shore-parallel elongated stromatolite mounds (Fig. 1A, B, D) are found on gently sloping platforms (2 m/km) in bights (Fig. 1C) (Jahnert and Collins, 2013). These mounds have a wavelength (the distance between two adjacent rows) of about 10 m and a width-to-wavelength ratio of about 0.3. Closer to shore, the shore-parallel mounds transition in few tens of meters to elongated forms that are shore-perpendicular (Fig. 1B) and have a narrower wavelength of ~2 m and a larger width-to-wavelength ratio of ~0.65 (Fig. S1, Supplementary Information). These differences in the geometry and

* Corresponding author.

http://dx.doi.org/10.1016/j.epsl.2014.04.036
0012-821X/

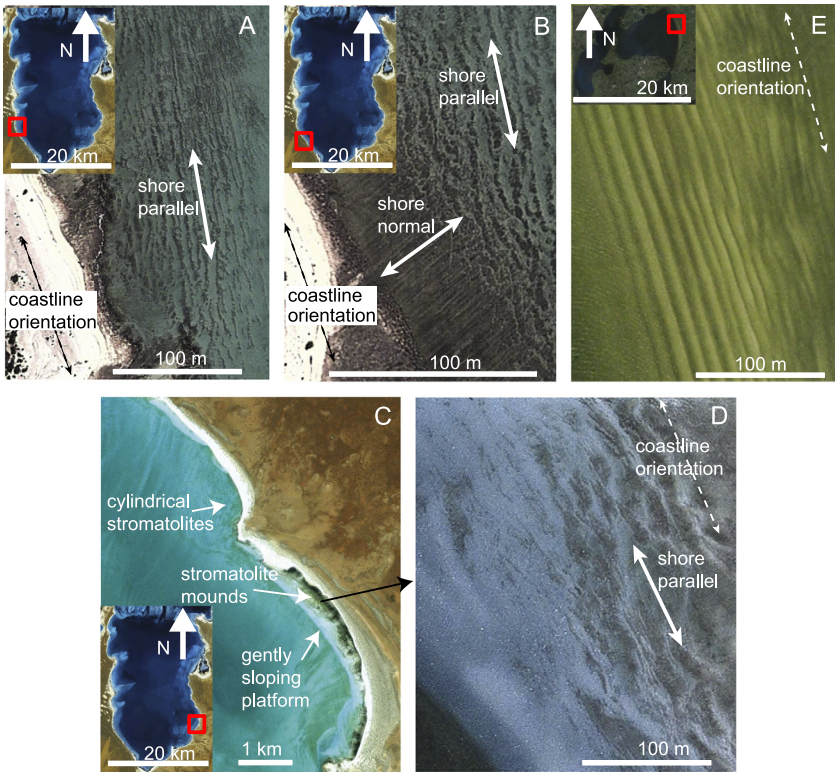

Fig. 1. Elongated features parallel to modern, gently-sloping coastlines. (A, B, D) Large elongated stromatolites are approximately parallel to the coastline in Hamelin Pool, Western Australia. These stromatolite mounds are about 2 m wide and have a wavelength (the distance between two consecutive rows) of about 10 m. Images from Google Earth (recorded 6/17/2012, DigitalGlobe). Note in (B) the presence of shore-normal elongated stromatolites with a wavelength of few meters in the upper intertidal area. (C) Cylindrical stromatolites are found at headlands characterized by a steep platform (40 m/km); stromatolite mounds are found at bights characterized by a gentle sloping platform (2 m/km) (Jahnert and Collins, 2013). Image from Google Earth (recorded 12/20/2006, DigitalGlobe). (E) Sand bars in Lovns Bredning Bay, Denmark, a bay similar in size to Hamelin Pool. Image from Google Earth (recorded 7/30/2005, Scankort).

orientation of stromatolites imply either that the currents change abruptly from shore-parallel to shore-normal, or that factors other than currents shape the widely spaced stromatolites on the gently sloping platform. Because the shore-parallel stromatolites in Hamelin Pool are approximately parallel to the prevailing wind direction, their formation has been attributed to an unknown wind-induced process (Playford and Cockbain, 1976), possibly a Langmuir circulation (Playford, 1980), which consists of helicoidal cells aligned with the wind direction at the water surface. However, Langmuir cells drift crosswind within tens of minutes (Gargett and Wells, 2007), i.e., much faster than the minimum time of a few weeks required to establish visible microbial mats that protect sandy sediments from erosion (Fang et al., 2013). Thus, factors responsible for the formation of elongated of stromatolites with a wavelength of approximately 10 m in Hamelin Pool, or even larger elongated stromatolite mounds in the geologic record (Truswell and Eriksson, 1973; Eriksson and Truswell, 1974; Hoffman, 1974; Young and Long, 1976; Beukes, 1987) remain unclear.

Here, we consider the similarity between shapes and sizes of modern sand bars and shore-parallel elongated stromatolites and hypothesize that interactions among microbes, waves and the motion of carbonate sediments on sand bars control the geometry of widely spaced, elongated, shore-parallel stromatolites. Intertidal sand bars, or sand waves as defined by Masselink et al. (2006), consist of elongated ridges and runnels that are generally parallel to the coastline, and are found in low wave energy settings characterized by gentle bed slopes (~10 m/km) and moderate fetches (5–50 km) (Evans, 1950; Dolan and Dean, 1985; Elgar et al., 2003; Masselink et al., 2006). Sand bars are regularly spaced, have a wavelength of 5–100 m and an amplitude of ~0.5 m, and can be found in configurations with tens of rows (Fig. 1E). Sand bars form through a positive feedback between hydrodynamics and morphodynamics. When a partially standing water wave is present over a flat bed, the Lagrangian drift near the bottom of the boundary layer converges toward the nodes and diverges from the antinodes of the surface wave, while the opposite occurs near the top of the boundary layer (Mei, 1985). As a consequence, sand grains transported as bed-load accumulate below the nodes, generating sand bars with a wavelength that is one half of the surface wave (O'Hare and Davies, 1990; Yu and Mei, 2000). If smaller particles are present and are transported in suspension, they accumulate below the wave antinodes (Landry et al., 2007). A feedback exists because standing or partially standing waves are generated by wave reflection over the sand bars (Davies, 1982; Mei, 1985; Heathershaw, 1982). For a fully standing wave, sand bars have ridges centered below the wave nodes, where the horizontal velocities are maximized, and runnels centered below the wave antinodes, where the horizontal velocities are minimized. For a partially standing wave, bar ridges and runnels are slightly shifted seaward with respect to the wave nodes and antinodes (Hancock et al., 2008).

We hypothesize that the lower shear stress, reduced sediment motion and accumulation of fine sediments in the runnels of carbonate sand bars can allow microbial growth and lithification in these areas. At the same time, sediment motion in sand bar ridges prevents microbial colonization. This spatial pattern of microbial growth initiates shore-parallel elongated stromatolites that form by microbial trapping and binding of sediments and lithification. We test this hypothesis by growing microbial mats on active sand bars in a laboratory setting. We perform experiments with a fully standing wave, and then apply a simplified hydrodynamic model to extend the results to the case of a partially standing wave. Finally

we propose a model that can explain the elongated morphology of some modern intertidal elongated stromatolites, as well as >10 m scale elongated mounds in the geologic record.

2. Methods

2.1. Experiment

We performed a laboratory experiment to determine how the flow and sediment transport that generate variegated sand bar topography influence the patterns of microbial colonization and growth. The experiment was conducted in a wave tank 120 cm long (L) and 0.3 m wide that was sterilized with 70% ethanol in nanopure water. Aragonite sand was sorted by sieving ($D_{50} = 254$ µm, $D_{10} = 171$ µm, $D_{90} = 382$ µm), autoclaved and spread into a flat, 5 cm thick layer that covered the entire bottom of the wave tank. Sterile seawater medium was gently poured into the tank to form a 15 cm deep (d) layer of water above the sand. This medium consisted of (in g/L of deionized water): 21.14 NaCl, 3.55 Na_2SO_4, 0.59 KCl, 0.17 $NaHCO_3$, 9.59 $MgCl_2{\cdot}6H_2O$, 1.34 $CaCl_2{\cdot}2H_2O$, 0.03446 $NaNO_3$, 0.00309 Na_3PO_4, 5 ml of trace element solution SL-10 without $FeCl_2$, 1 ml of vitamin solution (SL-10 and vitamin solution recipes in DSMZ medium 141, Braunschweig, Germany: Catalogue of strains 1993). Autoclaved nanopure water was added periodically to compensate for evaporation, and water temperature was kept around 20 °C. Two 18″ long fluorescent light tubes (Ultrasun superday light, 6500 K, ZooMed aquatic, Germany) were mounted on top of the tank and were operated with a 12 hour light-dark cycle, providing a quantum irradiance of ~50 µmol m^{-2} s^{-1} at the bed surface.

A standing wave was generated by forcing the water with a propeller mounted in a vertically oriented tube and connected to a well of ~1 dm^3 (Tunze Wavebox mini, Germany, modified with an elbow junction). The propeller was switched on and off with a constant period, equal to the second-mode longitudinal surface seiche period of the tank, $T = 2\pi/\sqrt{gk\tanh(kd)} = 1.1$ s, with a wave number $k = 2\pi/L$, generating a wave with an amplitude, a, equal to 3 cm, equivalent to a fully reflected wave with an incident wave amplitude, a_i, equal to $a/2$. The resulting standing wave had three antinodes, one at each end of the tank and one in the middle, and two nodes (Fig. 2B). The wave was present during the entire growth experiment (40 days), and was stopped for ~10 minutes each day to take pictures and take samples of mats and water chemistry.

During the first 24 hours, the very fine material (approximately <64 µm) was removed from the water column by a filter pump (D1, Vortex, FL, USA) to ensure water transparency. NaOH was added regularly to maintain a pH of ~8. The pH was monitored weekly (colorpHast pH indicator strips, EMD Millipore, Germany). Ca^{2+} concentration was monitored weekly by titration (Calcium test kit, API aquarium pharmaceutical, PA, USA). Minimum fluorescence yield, *Fo*, was measured with a PAM fluorometer (Diving-PAM, Walz, Germany). *Fo* was measured every centimeter along three transects parallel to the tank length, holding the instrument sensor ~5 mm above the bed surface. Dark adaptation was not necessary because light conditions were kept constant during all measurements. *Fo* was used as a proxy for the photosynthetic biomass in mats (Honeywill et al., 2002; Murphy et al., 2009), and was normalized to the range from 0, corresponding to the value of bare sand, to 1, corresponding to the maximum value measured during the experiment (Jesus et al., 2005).

A stationary bed pattern evolved in the sterile solution after three to four hours of wave activity (see Results). After the first 24 hours of wave activity, a 1 cm wide × 1 cm long × 0.3 cm thick piece of cyanobacterial mat was excised by a sterile scalpel knife from another tank, mechanically dispersed into

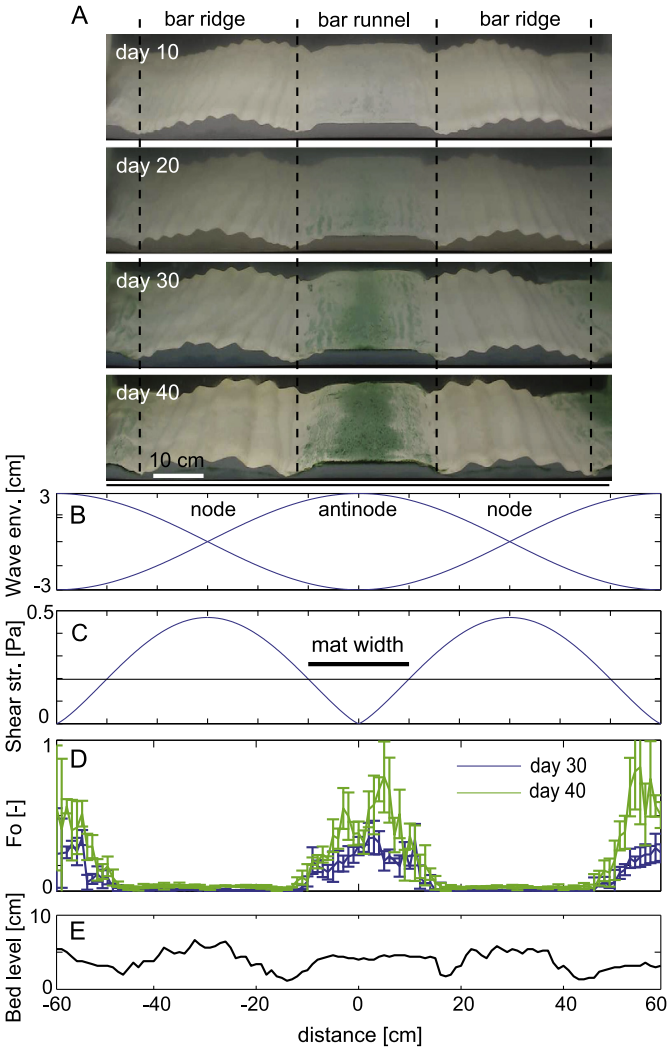

Fig. 2. Microbial mat growth in the laboratory wave tank. (A) Side views of the experiment at 10-day intervals. The runnels retained the initial bed elevation because the shear stress was below the critical value for sediment motion. (B) Standing wave envelope. (C) Calculated maximum bed shear stress. Note that spatial patterns in the calculated shear stress are caused by the modulation associated with the standing wave, not by the bed topography. Horizontal line marks the critical shear stress for the aragonite sand, 0.2 Pa, estimated using the Shields' formula, $\tau_{cr} = 0.047g(\rho_s - \rho_w)D_{50}$. (D) Normalized minimum fluorescence yield, *Fo*, used as a proxy for mat biomass (see methods). Error bars represent the standard deviation. *Fo* matches the patterns inferred visually from the photographs. (E) Bed elevation, measured at the end of day 1.

~1 mm^3 fragments, and distributed uniformly over the water surface in the wave tank. This mat, originally seeded with a sample taken from Cape Cod (MA, USA), was grown on the same carbonate substrate, in gently stirred medium under the same chemical and light conditions described above. Epifluorescence and transmitted-light microscopy (Axio Imager M1, Zeiss, Germany) revealed long, non-heterocystous, filamentous cyanobacteria as the primary producers in the thick mats from the runnels (see Results).

The experiment was monitored by time-lapse photography using a high resolution webcamera (HD Pro webcam 920, Logitech) mounted ~0.5 m from the tank and ~0.2 m above the bed level. Photographs of the sediment surface were taken manually with a digital camera held ~0.3 m above the bed. The experiment was repeated under identical conditions to test for reproducibility.

2.2. Partially standing wave hydrodynamics

We computed the bed shear stress as $\tau(x) = (1/2)\rho_w f_w(x) \times [U(x)]^2$, where $U(x) = 2\pi 2a_i/[T\sinh(kd)]|\sin(kx)|$ is the spatially

variable maximum bed orbital velocity, $f_w(x)$ is a spatially variable friction coefficient, estimated according to Nielsen (1992),

$$f_w(x) = \begin{cases} 0.04(A(x)/[3D_{50}])^{-1/4} & A_w(x)/3D_{50} > 100, \\ 0.4(A(x)/[3D_{50}])^{-3/4} & A_w(x)/3D_{50} \leq 100, \end{cases} \quad (1)$$

where $A(x) = TU(x)/[2\pi]$ is the spatially variable bed orbital amplitude; and x is the distance along the wave oscillation direction, with $x = 0$ located below a wave antinode. For the conditions in our experiment, we calculate the maximum bed orbital velocity, bed orbital amplitude and bed shear stress below the nodes as $U_{\text{node}} = 0.2$ m/s, $A_{\text{node}} = 3.5$ cm, and $\tau_{\text{node}} = 0.48$ Pa.

For partially standing waves, which are more common in natural environments than fully standing waves, the bed shear stress deviates from our simple experimental case. Specifically, partial reflection increases the bed shear stress below the antinodes. In the limiting case of fully propagating waves, no spatial modulation of the bed shear stress is present. For partially standing waves, linear wave theory predicts the shear stress field as a function of the reflection coefficient r, the amplitude of the reflected wave relative to the incident wave. The shear stress under partial wave reflection can be computed using a modified spatially variable maximum bed orbital velocity,

$$U(x) = 2\pi a_i / \left[T \sinh(kd)\right] \sqrt{4r\left[\sin(kx)\right]^2 + (1-r)^2}. \quad (2)$$

3. Results

3.1. Bed topography

The bed topography of sterile aragonite sand in the 1.2 m long wave tank resembled patterns reported in laboratory studies that generated standing waves in 10–20 m long tanks (Landry et al., 2007; Hancock et al., 2008) and the topography of natural, >10 m wide sand bars. Ridges approximately 2 cm tall formed below the nodes of the standing wave (Fig. 2A). The bed remained flat in the runnels under the antinodes of the standing wave. Areas ~1 cm lower than the initial flat bed formed at the boundaries between ridges and runnels. Ripples formed on the bar ridges and migrated back and forth by about a wavelength every few hours throughout the experiment (Video 1). The time-averaged ripple height and wavelength below the antinodes were 0.7 cm and 5 cm, respectively. These values remained approximately constant during the experiment (Fig. S2) and agreed with the predictions made by linear wave theory and semi-empirical equations for the geometry of ripples (Nielsen, 1981) (see Supplementary Information).

Ripples did not form in the runnels, where $a < 1$ mm thick layer of fine sediment grains (<64 μm) accumulated but bed load transport was negligible. This material was likely entrained into suspension on the ridges and preferentially deposited on the low-energy runnels, as reported in a previous study of sand bars (Landry et al., 2007). A few rows of mm-deep and cm-wide elongated ellipsoidal depressions formed after a few days at the edges of the runnels and persisted throughout the experiment (Fig. S3). The mechanism that formed these features is unknown, but it may be associated with the presence of very fine sediments and flow conditions close to the threshold for sediment motion.

3.2. Patterns of mat growth

Photosynthetic mats colonized the tank ~20 days after inoculation (Fig. 2A). The same timescale for colonization was observed in other laboratory experiments (Graba et al., 2010) and natural environments (Uehlinger et al., 1996). Mats grew in the runnels and produced two distinct patterns: a continuous ~10 cm wide band centered below each antinode; and multiple, 1 cm wide bands in the ellipsoidal depressions at the runnel edges (Fig. 2A, Fig. S3, Video 1). Less than 1 mm thin mats colonized the cm-wide ellipsoidal depressions at the edges of the runnels faster than the adjacent flat areas (Fig. S3). Unicellular cyanobacteria were abundant and filamentous forms were rare in these mats, the mats were friable and did not contain abundant trapped or precipitated mud. Because the presence of these depressions may be specific to our experiment, we focus our discussion primarily on the macroscopic difference between ridges and runnels. The runnels were covered by more than 1 mm thick, cohesive, tufted mats that contained abundant filamentous cyanobacteria. At day 40, filamentous cyanobacteria and the extrapolymeric matrix in the runnels were heavily coated by carbonate, suggesting that the trapping and binding of fines and cementation occurred within a few weeks.

Microbes did not grow on the ridges, where ripples constantly migrated back and forth, and a layer equal to the ripple height was reworked every few hours (Fig. 2A, Fig. S3, Video 1). Small fragments of mats remained suspended above the ridges during the entire experiment, but were unable to attach to the ripples or stabilize the bed. Mat growth was not observed in the rippled area on or below the sediment surface, suggesting that the surface measurements with the PAM fluorometer were good indicators of the total amount of microbial mat. Microbial colonization, visible ecology and coating by carbonate were replicated in a subsequent experiment (Fig. S4), suggesting that these patterns were robust and were not affected by small fluctuations in physical, chemical and biological parameters.

3.3. Expected mat colonization patterns and stromatolites morphology with partially standing waves

The width of microbial mats that colonized the bar runnels in our experiments coincided with the zone where shear stress remained below the critical value for grain motion (Fig. 2C). If the microbial mats trap and bind sediments, facilitate lithification through carbonate precipitation, and eventually build stromatolites, the incipient stromatolites will inherit the width of the mats. The spatially variable bed shear stress (Eq. (2)), combined with the Shields criterion, $\tau_{cr} = 0.047 g(\rho_s - \rho_w)D_{50}$, was used to predict the width of the area where mats grow, i.e. $\tau(x) < \tau_{cr}$, as a function of water depth, incident wave height, reflection coefficient, sediment grain size and sand bar wavelength, which is equal to half the water surface wavelength (Mei, 1985; Elgar et al., 2003) (Fig. 3).

According to our simplified model, elongated stromatolites can only form in sandy sediments without preexisting hard ground if some regions of the bed experience shear stress above the critical value for sediment motion and others experience shear stress below this value. For a wide range of reflection coefficients and wave heights, elongated stromatolites shaped by interactions between microbial mats and sand bars should have a small width-to-wavelength ratio (0.1–0.4, see Fig. 3). The width-to-wavelength ratio of modern shore-parallel elongated intertidal stromatolites in Hamelin Pool (Fig. 1A, Fig. S1) fall squarely within the range predicted by our model (Fig. 3). If the shear stress is everywhere smaller than the critical value for sediment motion, the bed will not develop any microbial growth pattern associated with sand bars (Fig. 3). Instead, microbial mats will form a uniform microbial pavement (Jahnert and Collins, 2013) and perhaps develop spatial patterns at scales much smaller than those of sand bars (e.g., Petroff et al., 2010; Sim et al., 2012). If the shear stress exceeds the critical value everywhere, microbial mats cannot colonize any portion of the bed and no stromatolites will form (Fig. 3). However, microbial mats would be able to grow and persist in areas that experience shear stresses above the critical value for abiotic sediment motion if the timescale for biostabilization is shorter than

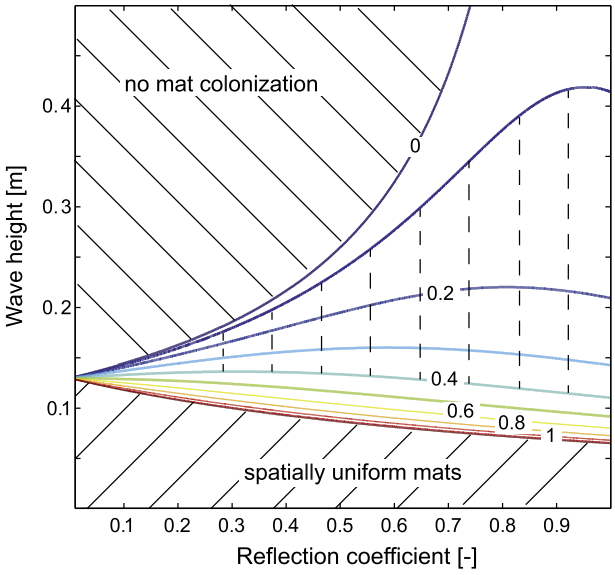

Fig. 3. Contour plot of the predicted ratio between mat width and sand bar wavelength as a function of the incident wave height, H_i, equal to twice the incident wave amplitude, a_i, and the reflection coefficient, r. Calculations were performed for a fixed water depth (1 m), sand bar wavelength (10 m), and sediment diameter ($D_{50} = 250$ μm), conditions that apply to Hamelin Pool. The region with vertical dashed lines indicates the width-to-wavelength ratio of the stromatolite mounds in Hamelin Pool.

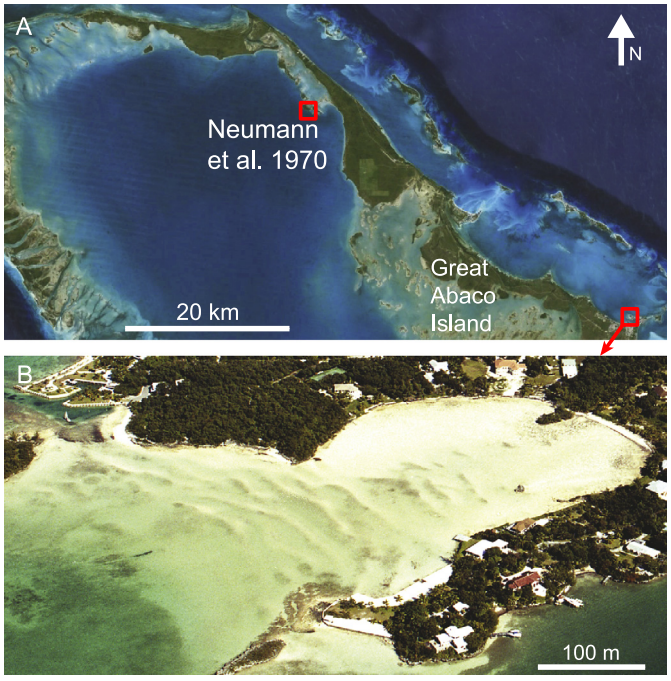

Fig. 4. Sites in the Bahamas with shore-parallel sand bars. (A) The top red square indicates the "basin harbor" site in Neumann et al. (1970), an embayment facing south-west; the bottom red square indicates an embayment with a shallow platform and a fetch of ~20 km. Image from Google Earth (accessed 4/9/2013, SIO, NOAA, U.S. Navy, NGA, GEBCO, NASA, Landsat). (B) This site shows darker areas in the sand bar runnels, possibly microbial mats. Note that the presumed mat growth occurs slightly landward of the bottom of the runnel, in the location where the wave antinodes are expected to be in the case of a partially standing wave (Hancock et al., 2008). Image from Aerial Only Gallery, published with permission. (For interpretation of the references to color in this figure legend, the reader is referred to the web version of this article.)

the timescale for the occurrence of sediment-reworking events (Mariotti and Fagherazzi, 2012). For example, laboratory experiments show that the biostabilization of ooid-rich sediments from the Bahamas by the already present microbial communities can occur in less than a day in the presence of quiet conditions (Paterson et al., 2008). As such, microbial mats would be able to colonize the runnels even though the shear stress there occasionally exceeds the critical value for abiotic sediment motion.

4. Discussion

4.1. Timescales and spatial patterns of hydrodynamic conditions and mat growth

Our experiment links the spatial patterns of mat growth to the heterogeneous hydrodynamic conditions that create ripples on the ridges of sand bars and flat beds or small ripples in the runnels (O'Hare and Davies, 1990; Elgar et al., 2003; Landry et al., 2007; Hale and McCann, 1982). Hydrodynamic disturbances that are strong enough to move barren sediments and frequent enough to prevent biostabilization during calm weather should prevent mat growth (Mariotti and Fagherazzi, 2012). In our experiment, mats were unable to colonize the sand bar ridges because ripples migrated and rearranged over hours, i.e., faster than the weeks-long time required for the mat to colonize and stabilize the surface. This experimental observation is consistent with the absence of mats from natural sediments that are often mobilized (Gebelein, 1969) and the destruction of thick mats by flows that can mobilize sand grains (Neumann et al., 1970).

Reduced shear stresses and sediment mobility allowed microbial growth in the sand bar runnels (Fig. 2D). These experimental results are consistent with the reported patterns of mat growth on sand bars in a shore platform partially exposed to a ~30 km wide shallow bank in Abaco, Bahamas (Fig. 4A) (Neumann et al., 1970). There, microbial mats were present in both ridges and runnels, but bar ridges contain coarser and better sorted sand than the runnels, and grain-to-grain adhesion was stronger in the runnels (Neumann et al., 1970). Our results imply that these Bahamian mats grew on both ridges and runnels during a prolonged period of reduced wave activity because high wave energy during storms would preferentially erode bar ridges, resulting in patterns similar to those found in our experiment. Importantly, even though seasonal storms may erode mats on the ridges, they are unlikely to alter the overall topography of sand bars. Because of a morphodynamic feedback (Mei, 1985), sand bars maintain their shape and position over several years (Dawson et al., 2002; Elgar et al., 2003; Yamada and Kobayashi, 2007) and up to tens of years (Neumann et al., 1970; Bathurst, 1971; Moore et al., 2003). The analogy between the microbial colonization patterns in the sand bars of the Abaco site in the Bahamas and Hamelin Pool is further supported by the similarity in wave exposure between the two sites. Both sites have shallow platforms facing fetches of about 20–30 km, even though lithification may be faster in the hypersaline Hamelin Pool. Examination of aerial photographs suggests the presence of similar, but currently unreported, colonization patterns on sand bars at other Bahamian sites characterized by a similar wave exposure (Fig. 4).

4.2. Stromatolite mounds in wave-dominated environments

The decadal persistence of sand bars suggests that stable, thick, resistant mats can form and lithify in sand bar runnels (Fig. 5A; Neumann et al., 1970). Indeed, our experiment shows that ~1 mm thick photosynthetic mats can colonize sand bar runnels in ~20 days. When these mats also facilitate the precipitation of carbonate minerals and cementation, the macroscopic patterns in mats should dictate the elongated morphology in incipient stromatolites (Fig. 5B). Cementation occurs over several months (Macintyre et al., 2000; Reid et al., 2000), slower than mat growth, but faster than the decadal migration of sand bars. Once microbially hardened

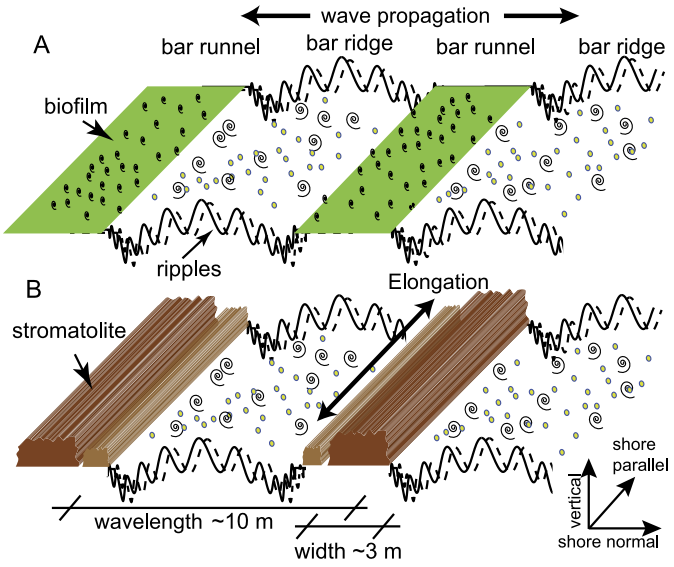

Fig. 5. Schematic diagram of stromatolite formation on sand bars. Whorls indicate elevated bed shear stress, dots indicate the presence of sediment motion, and undulating bed with shifting position indicates the presence of migrating ripples. (A) Mats grow on the sand bar runnels, where sediment motion is reduced. Sediment motion and ripple migration on the bar ridges prevent microbial colonization. (B) Mat growth and lithification leads to elongated stromatolite mounds that are perpendicular to the direction of wave propagation and parallel to the shoreline (Holthuijsen, 2007).

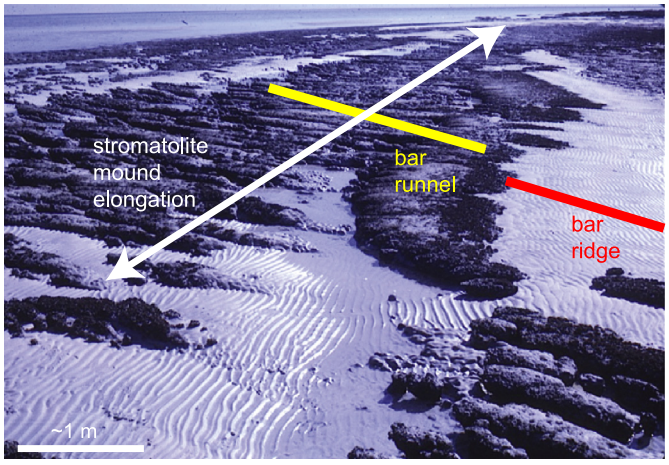

Fig. 6. Intertidal elongated stromatolite mounds parallel to the shoreline near Carbla Point in Hamelin Pool. The image was taken at low tide. High-tide shoreline is toward the right, and its orientation can be inferred from the water line in the upper part of the image. The presence of water and unconsolidated ripples suggest that this area is periodically submerged and experiences wave activity. Mounds are in bar runnels, about 10–30 cm below the adjacent ridges. Stromatolites are absent from the ridges. Note the presence of a secondary elongated morphology perpendicular to the mound orientation and characterized by a spacing of less than a meter. This shore-normal elongated morphology is likely controlled by tidal or wind-generated currents. Photo courtesy of P. Hoffman.

surfaces form, they can persist even after the sand bars disappear, withstand high energy conditions and intermittent sediment burial (Playford, 1980; Reid et al., 1995, 2000).

The preferential growth of mats on hard, lithified ground can eventually produce stromatolites that are higher than the about 0.5 m high adjacent sand bar ridges (Figs. 5B, 6). These emergent structures would behave as breakwaters, reduce the wave energy propagating shoreward (Kamphuis, 2000), and allow mat establishment in the sand bar ridges closest to the shoreline (Fig. 7). As a result, stromatolite rows would merge and form large stromatolite mounds, with widths equal to several wavelengths of

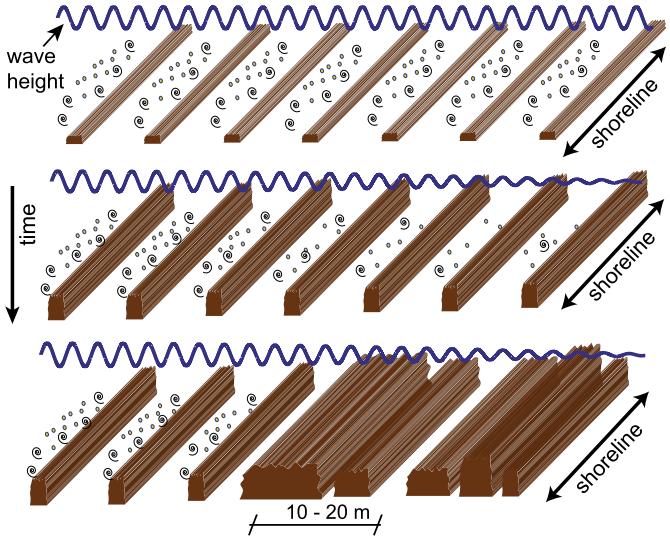

Fig. 7. Schematic diagram showing hypothesized formation of large elongated stromatolite mounds. Top: Shore-parallel elongated stromatolite mounds form in the sand bar runnel. Whorls indicate elevated bed shear stress, dots indicate the presence of sediment motion. Middle: Stromatolite emergence reduces the wave height reaching the shoreline. Bottom: Reduced sediment motion in the ridges leads to laterally merged stromatolites, creating larger (10–20 m wide) stromatolite mounds.

sand bars (Fig. 7). As mentioned above, merging might also occur through microbial colonization of areas that are reworked on a timescale that is shorter than the timescale for biostabilization (Mariotti and Fagherazzi, 2012), a condition promoted by the presence of fast-growing organisms and seawater chemistry that favors carbonate precipitation. In Hamelin Pool, elongated stromatolites with barren interspaces are common on the intertidal platform, whereas wider, shore-parallel, elongated mounds are present toward the landward end of the platform (Figs. 1D, 8A). This suggests that the wider mounds might have developed as elongated stromatolites widened and merged. Merging of shore-parallel elongated stromatolites may also be responsible for the formation of some large stromatolite mounds observed in the geologic record (Fig. 8B) (Truswell and Eriksson, 1973; Hoffman, 1974; Young and Long, 1976; Beukes, 1987; Eriksson and Truswell, 1974). It should be noted that our model explains only the large scale (>1 m) morphology of stromatolite mounds. Hydro-sedimentary interactions and other processes such as lithification and diagenesis will likely impact the intermediate scale (0.1–1 m) morphologies of stromatolite mounds. Indeed, few decimeters wide shore-perpendicular elongated columns develop on some elongated mounds in Hamelin Pool (Fig. 6), probably through interactions with tidal or wind-generated currents (Logan, 1961; Hoffman, 1967).

Our model predicts that at least some areas between elongated stromatolite mounds should contain wave-generated ripples, remnants of the former sand bar ridges (Figs. 2A, 4B). Because both sand bars and ripples are generated by waves propagating perpendicularly to the shoreline, ripple crests and stromatolite mounds should be parallel to each other and to the shoreline. This seems to be the case in Hamelin Pool (Playford, 1980) (Fig. 6). Wave ripples are also reported in the same facies as large elongated stromatolite mounds (Truswell and Eriksson, 1973; Eriksson and Truswell, 1974; Beukes, 1987), but the current lack of information about the relative orientations of the mounds and ripple crests prevents further comparisons between the sand bar initiation model and these old stromatolites. If the role of sand bars in the formation of past stromatolites is recognized, this further constrains the water depth, shear stresses and morphology

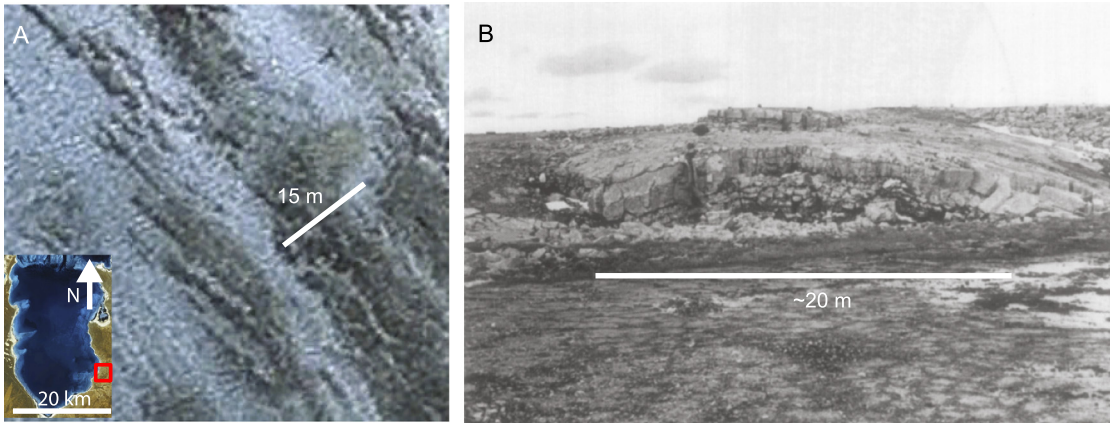

Fig. 8. (A) Large (10–20 m wide) shore-parallel stromatolite mounds in Hamelin Pool, showing the presence of narrower elongated stromatolites. (B) Outcrop of a Precambrian elongated stromatolite mound in the Reynolds Point Formation, Victoria Island, Canada. View is roughly parallel to the direction of elongation. Image from Young and Long (1976).

of the platforms on which stromatolites formed (Masselink et al., 2006).

Stromatolites that contain trapped and bound sediment grains must require facies characterized by sediment reworking. This may seem paradoxical, because microbial mats do not establish where sediments are often mobilized (Gebelein, 1969). Our study of mat growth on sand bars provides one example that reconciles this paradox, showing that large bedform patterns can both inhibit and foster microbial mat growth at different locations on the bed and provide a template for stromatolite growth. Analogous conditions that selectively allow mat establishment in the presence of sand transport could be responsible for stromatolites with other morphologies, such as the wide (~1 m diameter), cylindrical stromatolites observed on wave-swept beds covered with actively migrating sand ripples in areas with steep platforms within Hamelin Pool (Jahnert and Collins, 2013), and in some embayments in the Exuma Cays, Bahamas (Reid et al., 1995).

5. Conclusions

Interactions between wave motion, transport of carbonate sand, topography of the sand bed, and microbial mat growth were investigated in a laboratory experiment. This system reproduced the topography of sand bars and suggested a mechanism by which spatial patterns of bed shear stress and sediment motion might control meter-scale spatial patterns of microbial growth. Mats colonized sand bar runnels, where bed shear stresses are low and little sediment motion takes place, but not sand bar ridges, where ripples migrated and shear stresses were high. This growth pattern appears to have set the template for subsequent stromatolite growth. The sand bar mechanism is consistent with the scales, elongated morphology and shore-parallel orientation of meter-wide, elongated stromatolites in Hamelin Pool, Western Australia, and also may have initiated some large, >10 m-wide, elongated stromatolite mounds in the geologic record. The proposed model for the formation of elongated stromatolite mounds enhances the understanding of coupled physical, biological and chemical processes that shape stromatolites and the use of macroscopic stromatolite morphologies to characterize early life and its host environments.

Acknowledgements

G.M. and T.B. were supported by NASA Astrobiology Institute award NNA13AA90A, and NASA Exobiology award 6927184. G.M. was supported by a W.O. Crosby Postdoctoral Fellowship. J.T.P. was supported by the NSF Geomorphology and Land Use Dynamics Program under award EAR-1225865.

Appendix A. Supplementary material

Supplementary material related to this article can be found online at http://dx.doi.org/10.1016/j.epsl.2014.04.036.

References

Altermann, W., 2008. Accretion, trapping and binding of sediment in Archean stromatolites—morphological expression of the antiquity of life. Space Sci. Rev. 135, 55–79.

Bathurst, R.G.C., 1971. Carbonate Sediments and Their Diagenesis. Elsevier, Amsterdam, pp. 1–620.

Beukes, N.J., 1987. Facies relations, depositional environments and diagenesis in a major early Proterozoic stromatolitic carbonate platform to basinal sequence, Campbellrand Subgroup, Transvaal Supergroup, Southern Africa. Sediment. Geol. 54 (1–2), 1–46. http://dx.doi.org/10.1016/0037-0738(87)90002-9.

Bosak, T., Knoll, A.H., Petroff, A.P., 2013a. The meaning of stromatolites. Annu. Rev. Earth Planet. Sci. 41, 21–44.

Bosak, T., Mariotti, G., Perron, J.T., Macdonald, F.A., Pruss, S.B., 2013b. Microbial sedimentology of stromatolites in the Neoproterozoic cap carbonates. In: Ecosystem Paleobiology and Geobiology. In: Paleontological Special Papers, vol. 19. Paleontological Society, pp. 51–77.

Davies, A.G., 1982. The reflection of wave energy by undulations on the seabed. Dyn. Atmos. Ocean. 6 (4), 207–232. http://dx.doi.org/10.1016/0377-0265(82)90029-X.

Dawson, J.C., Davidson-Arnott, R.G.D., Ollerhead, J., 2002. Low-energy morphodynamics of a ridge and runnel system. J. Coast. Res. 36, 198–215.

Dolan, T.J., Dean, R.G., 1985. Multiple longshore sand bars in the upper Chesapeake Bay. Estuar. Coast. Shelf Sci. 21 (5), 727–743. http://dx.doi.org/10.1016/0272-7714(85)90069-1.

Elgar, S., Raubenheimer, B., Herbers, T.H.C., 2003. Bragg reflection of ocean waves from sandbars. Geophys. Res. Lett. 30 (1), 16.1–16.4. http://dx.doi.org/10.1029/2002GL016351.

Eriksson, K.A., Truswell, J.F., 1974. Tidal flat associations from a lower Proterozoic carbonate sequence in South Africa. Sedimentology 21 (2), 293–309. http://dx.doi.org/10.1111/j.1365-3091.1974.tb02060.x.

Evans, O.F., 1950. The low and ball of the Eastern Shore of Lake Michigan. J. Geol. 48 (5), 476–511.

Fang, H., Shang, Q., Chen, M., He, G., 2013. Changes in the critical erosion velocity for sediment colonized by biofilm. Sedimentology 61 (3), 648–659. http://dx.doi.org/10.1111/sed.12065.

Gargett, A.E., Wells, J.R., 2007. Langmuir turbulence in shallow water. Part 1. Observations. J. Fluid Mech. 576, 27–61. http://dx.doi.org/10.1017/S0022112006004575.

Gebelein, C.D., 1969. Distribution, morphology, and accretion rate of recent subtidal algal stromatolites, Bermuda. J. Sediment. Res. 39 (1), 49–69. http://dx.doi.org/10.1306/74D71BE0-2B21-11D7-8648000102C1865D.

Graba, M., Moulin, F., Boulêtreau, S., Garabétian, F., Kettab, A., Eiff, O., Sánchez-Pérez, J.M., Sauvage, S., 2010. Effect of near-bed turbulence on chronic detachment of epilithic biofilm: experimental and modeling approaches. Water Resour. Res. 46 (W11531).

Hale, P.B., McCann, S.B., 1982. Rhythmic topography in a mesotidal, low-wave-energy environment. J. Sediment. Res. 52 (2), 415–429. http://dx.doi.org/10.1306/212F7F6D-2B24-11D7-8648000102C1865D.

Hancock, M.J., Landry, B.J., Mei, C.C., 2008. Sandbar formation under surface waves: theory and experiments. J. Geophys. Res., Oceans 113 (C7). http://dx.doi.org/10.1029/2007JC004374.

Heathershaw, A.D., 1982. Seabed-wave resonance and sand bar growth. Nature 296 (5855), 343–345. http://dx.doi.org/10.1038/296343a0.

Hoffman, P., 1967. Algal stromatolites: use in stratigraphic correlation and paleocurrent determination. Science 157 (3792), 1043–1045. http://dx.doi.org/10.1126/science.157.3792.1043.

Hoffman, P., 1974. Shallow and deepwater stromatolites in lower Proterozoic platform-to-basin facies change, Great Slave Lake, Canada. Am. Assoc. Pet. Geol. Bull. 58 (5), 856–867.

Holthuijsen, L.H., 2007. Waves in Oceanic and Coastal Waters. Cambridge University Press, Cambridge, UK, pp. 1–404.

Honeywill, C., Paterson, D.M., Hagerthey, S., 2002. Determination of microphytobenthic biomass using pulse-amplitude modulated minimum fluorescence. Eur. J. Phycol. 37 (4), 485–492. http://dx.doi.org/10.1017/S0967026202003888.

Jahnert, R.J., Collins, L.B., 2013. Characteristics, distribution and morphogenesis of subtidal microbial systems in Shark Bay, Australia. Mar. Geol. (ISSN 0025-3227) 303–306 (15), 115–136. http://dx.doi.org/10.1016/j.margeo.2012.02.009.

Jefferson, C.W., Young, G.M., 1989. Late Proterozoic orange-weathering stromatolite biostrome Mackenzie Mountains and Western Arctic Canada. Reefs, Canada and Adjacent Area. In: Geldsetzer, H.H.J., James, N.P., Tebbutt, G.E. (Eds.), Canadian Society of Petroleum Geologists Memoirs, vol. 13, pp. 72–80.

Jesus, B., Brotas, V., Marani, M., Paterson, D.M., 2005. Spatial dynamics of microphytobenthos determined by PAM fluorescence. Estuar. Coast. Shelf Sci. 65 (1–2), 30–42. http://dx.doi.org/10.1016/j.ecss.2005.05.005.

Kamphuis, J.W., 2000. Introduction to Coastal Engineering and Management. World Scientific, Singapore, pp. 1–564.

Landry, B.J., Hancock, M.J., Mei, C.C., 2007. Note on sediment sorting in a sandy bed under standing water waves. Coast. Eng. 54 (9), 694–699. http://dx.doi.org/10.1016/j.coastaleng.2007.02.003.

Logan, B.W., 1961. Cryptozoon and associate stromatolites from the recent, Shark Bay, Western Australia. J. Geol. 69, 517–533. http://dx.doi.org/10.1086/626769.

Macintyre, I.G., Prufert-Bebout, L., Reid, R.P., 2000. The role of endolithic cyanobacteria in the formation of lithified laminae in Bahamian stromatolites. Sedimentology 47 (5), 915–921. http://dx.doi.org/10.1046/j.1365-3091.2000.00327.x.

Mariotti, G., Fagherazzi, S., 2012. Modeling the effect of tides and waves on benthic biofilms. J. Geophys. Res., Biogeosci. 117 (G4). http://dx.doi.org/10.1029/2012JG002064.

Masselink, G., Kroon, A., Davidson-Arnott, R.G.D., 2006. Morphodynamics of intertidal bars in wave-dominated coastal settings – A review. Geomorphology 73 (1–2), 33–49. http://dx.doi.org/10.1016/j.geomorph.2005.06.007.

Mei, C., 1985. Resonant reflection of surface-water waves by periodic sandbars. J. Fluid Mech. 152 (3), 315–335. http://dx.doi.org/10.1017/S0022112085000714.

Moore, L.J., Sullivan, C., Aubrey, D.G., 2003. Interannual evolution of multiple longshore sand bars in a mesotidal environment, Truro, Massachusetts, USA. Mar. Geol. 196 (3–4), 127–143. http://dx.doi.org/10.1016/S0025-3227(03)00028-8.

Murphy, R.J., Tolhurst, T.J., Chapman, M.G., Underwood, A.J., 2009. Seasonal distribution of microphytobenthos on mudflats in New South Wales, Australia measured by field spectrometry and PAM fluorometry. Estuarine. Coastal and Shelf Science 84, 108–118.

Neumann, A.C., Gebelein, C.D., Scoffin, T.P., 1970. The composition, structure and erodability of subtidal mats, Abaco, Bahamas. J. Sediment. Res. 40 (1), 274–297. http://dx.doi.org/10.1306/74D71F2D-2B21-11D7-8648000102C1865D.

Nielsen, P., 1981. Dynamics and geometry of wave-generated ripples. J. Geophys. Res., Oceans 86 (C7), 6467–6472. http://dx.doi.org/10.1029/JC086iC07p06467.

Nielsen, P., 1992. Coastal Bottom Boundary Layers and Sediment Transport. World Scientific Publishing Company, Singapore, pp. 1–340.

O'Hare, T.J., Davies, A.G., 1990. A laboratory study of sand bar evolution. J. Coast. Res. 6 (3), 531–544. http://dx.doi.org/10.2307/4297716.

Paterson, D.M., Aspden, R.J., Visscher, P.T., Consalvey, M., Andres, M.S., Decho, A.W., Stolz, J., Reid, R.P., 2008. Light-dependent biostabilisation of sediments by stromatolite assemblages. PLoS ONE 3 (9).

Petroff, A.P., Sim, M.S., Maslov, A., Krupenin, M., Rothman, D.H., Bosak, T., 2010. Biophysical basis for the geometry of conical stromatolites. Proc. Natl. Acad. Sci. USA 107, 9956–9961.

Playford, P.E., 1980. Environmental controls on the morphology of modern stromatolites at Hamelin Pool, Western Australia. In: Western Australian Geological Survey Annual Report for 1979, pp. 73–77.

Playford, P.E., Cockbain, A.E., 1976. Modern algal stromatolites at Hamelin Pool, a hypersaline barred basin in Shark Bay, Western Australia. In: Walter, M.R. (Ed.), Developments in Sedimentology. Elsevier, pp. 389–411, Chapter 8.2.

Reid, D.R.P., Macintyre, D.I.G., Browne, D.K.M., Steneck, D.R.S., Miller, D.T., 1995. Modern marine stromatolites in the Exuma Cays, Bahamas: uncommonly common. Facies 33 (1), 1–17. http://dx.doi.org/10.1007/BF02537442.

Reid, R.P., Visscher, P.T., Decho, A.W., Stolz, J.F., Bebout, B.M., Dupraz, C., Macintyre, I.G., Paerl, H.W., Pinckney, J.L., Prufert-Bebout, L., Steppe, T.F., DesMarais, D.J., 2000. The role of microbes in accretion, lamination and early lithification of modern marine stromatolites. Nature 406 (6799), 989–992. http://dx.doi.org/10.1038/35023158.

Sakurai, Y., Ito, M., Ueno, Y., Kitajima, K., Maruyama, S., 2005. Facies architecture and sequence-stratigraphic features of the Tumbiana Formation in the Pilbara Craton, northwestern Australia: implications for depositional environments of oxygenic stromatolites during the Late Archean. Precambrian Res. 138, 255–273.

Sim, M.S., Liang, B., Petroff, A.P., Evans, A., Klepac-Ceraj, V., Flannery, D.T., Walter, M.R., 2012. Oxygen-dependent morphogenesis of modern clumped photosynthetic mats and implications for the Archean stromatolite record. Geosciences 2, 235–259.

Tice, M.M., Thornton, D.C., Pope, M.C., Olszewski, T.D., Gong, J., 2011. Archean microbial mat communities. Annu. Rev. Earth Planet. Sci. 39, 297–319.

Truswell, J., Eriksson, K., 1973. Stromatolitic associations and their paleoenvironmental significance: a re-appraisal of a lower Proterozoic locality from northern Cape province, South Africa. Sediment. Geol. 10 (1), 1–23. http://dx.doi.org/10.1016/0037-0738(73)90008-0.

Uehlinger, U., Buhrer, H., Reichert, P., 1996. Periphyton dynamics in a flood-prone prealpine river: evaluation of significant processes by modelling. Freshw. Biol. 36 (2), 249–263. http://dx.doi.org/10.1046/j.1365-2427.1996.00082.x.

Yamada, F., Kobayashi, N., 2007. Intertidal multiple sand bars in a low-energy environment. J. Waterw. Port Coast. Ocean Eng. 133 (5), 343–351. http://dx.doi.org/10.1061/(ASCE)0733-950X(2007)133:5(343).

Young, G.M., Jefferson, C.W., 1975. Late Precambrian shallow water deposits, banks and Victoria Islands, Arctic Archipelago. Can. J. Earth Sci. 12 (10), 1734–1748. http://dx.doi.org/10.1139/e75-154.

Young, G.M., Long, D.G.F., 1976. Stromatolites and basin analysis: an example from the upper Proterozoic of northwestern Canada. Palaeogeogr. Palaeoclimatol. Palaeoecol. 19 (4), 303–318. http://dx.doi.org/10.1016/0031-0182(76)90031-6.

Yu, J., Mei, C.C., 2000. Formation of sand bars under surface waves. J. Fluid Mech. 416, 315–348. http://dx.doi.org/10.1017/S0022112000001063.